Ground-State Properties of Metallic Solids from *Ab Initio* Coupled-Cluster Theory

Verena A. Neufeld,*,† Hong-Zhou Ye,† and Timothy C. Berkelbach*,†,‡

†*Department of Chemistry, Columbia University, New York, New York 10027, USA*

‡*Center for Computational Quantum Physics, Flatiron Institute, New York, New York 10010, USA*

E-mail: verena.a.neufeld@gmail.com; tim.berkelbach@gmail.com

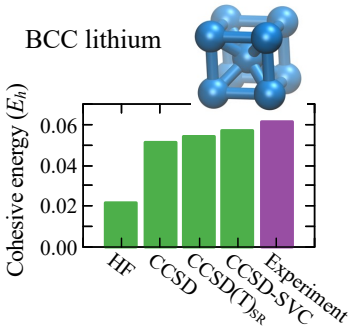

TOC graphic

Abstract

Metallic solids are an enormously important class of materials, but they are a challenging target for accurate wavefunction-based electronic structure theories and have not been studied in great detail by such methods. Here, we use coupled-cluster theory with single and double excitations (CCSD) to study the structure of solid lithium and aluminum using optimized Gaussian basis sets. We calculate the equilibrium lattice constant, bulk modulus, and cohesive energy and compare them to experimental values, finding accuracy comparable to common density functionals. Because the quantum chemical "gold standard" CCSD(T) (CCSD with

perturbative triple excitations) is inapplicable to metals in the thermodynamic limit, we test two approximate improvements to CCSD, which are found to improve the results.

Introduction. *Ab initio* wavefunction-based electronic structure theories are being increasingly applied to periodic solids,[1–13] where they can be used as predictive tools on their own or to guide the choice of functionals in more affordable density functional theory (DFT)[14,15] calculations. To date, most applications of these methods are to semiconducting or insulating systems. To realize their full predictive power, these methods must be extended to metals, which are essential in innumerable technologies, including energy storage and catalysis. This extension is a challenge because many of the most successful wavefunction-based methods employ finite-order perturbation theory, whose correlation energy typically diverges in the thermodynamic limit.[3,16–18] Coupled-cluster (CC) theory[19] is particularly promising in this regard, because even its lowest-order nontrivial truncation to single and double excitations (CCSD) includes a number of important, canonical classes of diagrams, including ladder diagrams (important at low density) and ring diagrams (important at high density and necessary to remove the aforementioned divergence).[20–24] Despite extensive application to the ground state of the uniform electron gas (UEG),[17,18,21–23,25–31] CC theory has seen limited application to atomistic metals.[8,32–35]

Here, we apply CCSD to study the structural and energetic properties of two simple metals, body-centered cubic (BCC) lithium and face-centered cubic (FCC) aluminum. We address two of the key technical hurdles associated especially with the *ab initio* study of metals, namely the removal of basis set error and finite-size error. To address basis set error, we use system-specific Gaussian-type orbital (GTO) basis sets[36,37] that are optimized to lower the total energy and to lower the condition number of the overlap matrix. We demonstrate the success of this approach by comparing our results to those obtained with plane-wave basis sets. To address finite-size error, we employ relatively dense Brillouin zone samplings with twisted boundary conditions and subsequent extrapolation. We then address the CCSD error by two approximate methods: adding the correlation energy due to perturbative triples[38] with a coarse Brillouin zone sampling or scaling the CCSD correlation energy by a non-empirical factor determined by the UEG.

Methods. For BCC Li, we use an isotropic primitive cell containing two atoms. For FCC Al, we use two unit cells: an anisotropic primitive cell containing two atoms and an isotropic

cubic cell with four atoms. Except where indicated, calculations were performed with the lattice constants $a = 3.5$ Å (Li) and $a = 4.05$ Å (Al), which are close to the experimental values. All calculations are performed at zero temperature using PySCF[6,39,40] (versions 1.7 and 2.0, as well as development versions) with libcint,[41] and GTO-based calculations were performed with Gaussian density fitting.[42–44] We use GTH pseudopotentials,[45–48] correlating three electrons per atom, for both Li and Al.

Basis set optimization. The original GTO basis sets designed for use with GTH pseudopotentials[37] were not optimized for correlated calculations and furthermore only contain s, p, and d functions. Therefore in this work, we re-optimize the GTH-DZVP (DZ), GTH-TZV2P (TZ), and GTH-QZV3P (QZ) basis sets; for aluminum, we also added f functions to the TZ and QZ basis sets, which were found to be important in our testing. In periodic solids, increasing the size of the basis set by brute force frequently leads to linear dependencies, quantified by an overlap matrix with large condition number, and concomitant numerical issues. Following similar works,[37,49–52] here we optimize these basis functions for each solid by minimizing the cost function

$$\text{cost} = E_{\text{HF}} + E_{\text{c}}^{(2)} + \gamma \ln(\text{cond}(\mathbf{S})) \tag{1}$$

where E_{HF} is the Hartree-Fock (HF) energy, $E_{\text{c}}^{(2)}$ is the second-order Møller-Plesset perturbation theory (MP2)[53] correlation energy, $\mathbf{S}$ is the periodic overlap matrix of the GTO basis, and $\gamma = 10^{-4}\ E_h$. For this basis set optimization, we sampled the Brillouin zone with a uniform mesh[54] of $N_{\boldsymbol{k}} = 2^3$ $\boldsymbol{k}$-points (Li) or $N_{\boldsymbol{k}} = 1^3$ $\boldsymbol{k}$-points (Al), including the Γ point; with these boundary conditions, the system is gapped and thus MP2 provides a well-defined and computationally affordable correlation energy. At this level of theory, the exponents and contraction coefficients of the GTO basis functions were optimized in an approximately alternating fashion. The optimization was started from the original GTH basis set (with additional f functions in TZ and QZ, for Al) and the final basis functions may represent a local minimum of the cost function. To avoid biasing the atomic structure, the cost function (1) was summed over

three lattice parameters approximately spanning the range used in later calculations. See the Supporting Information (SI) for further details about pseudopotentials and our optimized basis sets. The optimized basis sets are also available for download in machine-readable format at https://github.com/verena-neufeld/2022_data_for_paper_cc_al_li, along with data produced in this work.

To demonstrate the impact of basis set optimization, in Fig. 1 we show the basis set convergence of the MP2 and CCSD correlation energy of lithium and aluminum at the Γ point of their primitive cells, comparing GTO and plane wave (PW) results (for this figure only, the GTO results were evaluated using a PW basis set to compute the occupied bands and an approximate PW resolution of the original and optimized GTO bases to compute the virtual bands[50,55,56]). For Li, we see that GTO optimization increases the correlation energy by almost a factor of two, i.e., about 20 mE_h. A crude extrapolation suggests that the optimized QZ results recover about 80–90% of the correlation energy in the basis set limit. With this small $\boldsymbol{k}$-point mesh, we can perform PW calculations with a reasonably large number of orbitals, but for Li these results converge slowly due to the inclusion of the core 1s electrons. An MP2 calculation with our optimized QZ basis set with 67 bands recovers more correlation energy than one with a PW basis set containing 1203 orbitals, highlighting the immense computational savings afforded by GTO basis sets. With very large PW basis sets, we begin to see the onset of N_{bands}^{-1} convergence to a basis set limit in good agreement with that of the optimized GTO basis sets. For Al, the core electrons are not explicitly treated in the calculations and the PW calculations converge faster. Again, we see the benefit of basis set optimization as well as the addition of f functions. The QZ result captures about 90% of the correlation energy in the basis set limit.

In addition to recovering a greater amount of electron correlation, our basis sets were optimized to reduce their numerically problematic linear dependencies. Indeed, with our largest QZ basis, the condition number of the overlap matrix decreases from about 10^{13} to 10^4 for Li and from about 10^{16} to 10^7 for Al. For both Li and Al, the qualitative similarity between the MP2 and CCSD correlation energies justifies our use of the former when optimizing the GTO basis set and suggests

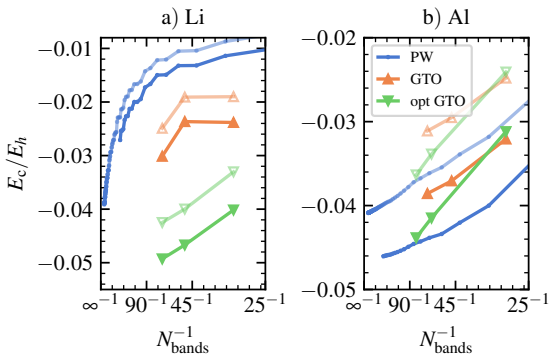

Figure 1: Basis set convergence of MP2 (faint, open symbols) and CCSD (solid, closed symbols) correlation energies E_c per atom for (a) lithium and (b) aluminum. Results were obtained using plane waves (PW) of increasing energy and using Gaussian type orbitals (GTO) and optimized GTOs, at the DZ, TZ, and QZ level. The Brillouin zone was sampled only at the Γ point.

good transferability to other correlated methods.[50]

Henceforth, we use these re-optimized GTO basis sets. Compared to the transferable, correlation-consistent basis sets recently developed by two of us,[56] preliminary testing (not shown) indicates that these optimized GTO basis sets exhibit slightly different basis set convergence but yield CBS results in good agreement.

Finite-size effects. Finite-size errors are especially problematic for metals due to shell-filling effects, which can be alleviated with twisted boundary conditions.[18,30,34,35,57–61] In Fig. 2, we show the finite-size convergence of the HF energy and CCSD correlation energy for Li and Al in the optimized DZ bases. HF calculations were performed with up to $N_{\boldsymbol{k}} = 8^3$ (Li) and $N_{\boldsymbol{k}} = 7^3$ (Al) $\boldsymbol{k}$-points, and a Madelung constant correction was used to eliminate the leading-order $N_{\boldsymbol{k}}^{-1/3}$ finite-size error[54,62,63] due to nonlocal exchange. All calculations were performed using a twisted boundary condition defined by the Baldereschi point,[57,59,61] which was found to yield smoother convergence to the thermodynamic limit (TDL) than calculations without a twist angle. Results for Li obtained by averaging over four Chadi-Cohen twist angles[58] (not shown) were found to give very similar results.

In this manner, the TDL of the HF energies can be estimated to an accuracy of about 1 mE_h. For Li, CCSD calculations were performed with up to $N_{\boldsymbol{k}} = 4^3$ $\boldsymbol{k}$-points; with that mesh they were performed using a truncated basis of MP2 natural orbitals and corrected based on results obtained

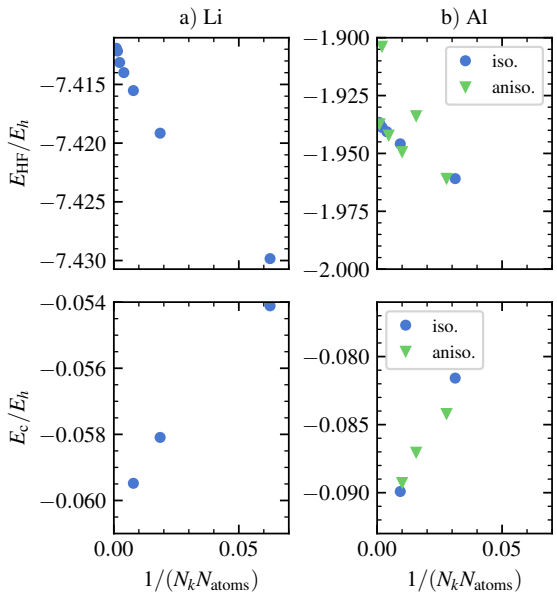

Figure 2: Thermodynamic limit convergence of the DZ HF (top) and DZ CCSD correlation (bottom) energy per atom as a function of the inverse of the number of atoms in the effective supercell $N_{\boldsymbol{k}} N_{\mathrm{atoms}}$, where $N_{\boldsymbol{k}}$ is the number of $\boldsymbol{k}$-points sampled in the Brillouin zone and N_{atoms} is the number of atoms in the unit cell. For Al, the results using an anisotropic primitive and an isotropic cubic cell are shown.

with smaller meshes. Extrapolation assuming finite-size errors that scale as $N_{\boldsymbol{k}}^{-1}$ suggests an extrapolation uncertainty of about 1 mE_h. For Al, due to the larger number of atoms in a cubic unit cell, our largest mesh has $N_{\boldsymbol{k}} = 3^3$ $\boldsymbol{k}$-points. For better extrapolation, we also performed calculations using an anisotropic primitive cell, with up to $N_{\boldsymbol{k}} = 5 \times 5 \times 2$. Except for two meshes, all results from both cell choices are found to lie roughly on a straight line and reliable extrapolation can be performed to estimate the HF energy in the TDL. With the anisotropic cell, two meshes ($4 \times 4 \times 2$ and $8 \times 8 \times 4$) yield HF energies that are too high, which may correspond to incorrect HF solutions due to the challenge of minimization in metals at zero temperature; somewhat surprisingly, the correlation energy associated with the higher-energy HF solution at $N_{\boldsymbol{k}} = 4 \times 4 \times 2$ is in line with the other correlation energies, facilitating extrapolation. In all future calculations on Al, we use the isotropic cell for HF energies and the anisotropic cell for correlation energies. The total energies that we calculate using our largest meshes differ from the extrapolated results by about 1 mE_h (Li) and 3-4 mE_h (Al), and the extrapolated results have an uncertainty of about 1 mE_h or less.

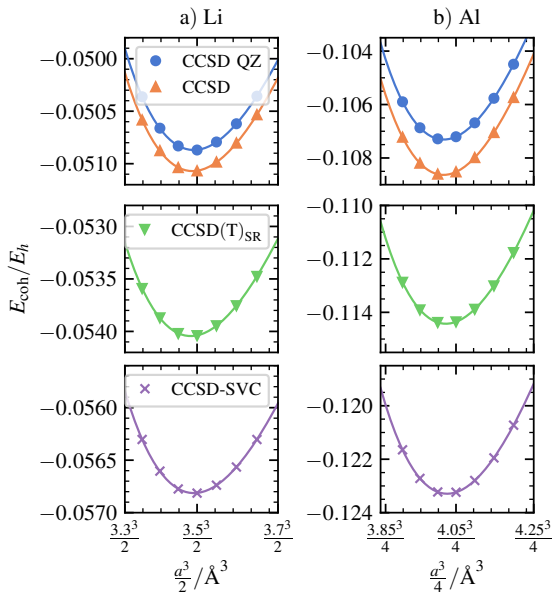

Figure 3: Cohesive energy equations of state from the indicated CCSD-based methods for (a) lithium and (b) aluminum. The Birch–Murnaghan equation[64,65] was fit to the data and shown as a solid line.

To our DZ results obtained with increasingly large $N_{\boldsymbol{k}}$, we add basis set corrections determined by calculations with smaller values of $N_{\boldsymbol{k}}$. For the HF energy, we assume that the QZ result is near the complete basis set (CBS) limit. For the correlation energy, the CBS limit is estimated via X^{-3} extrapolation[66] of TZ and QZ results, where $X = 3, 4$ is the cardinality.

Henceforth, we assume basis set corrections and finite-size corrections are independent and additive, enabling a composite approach to the estimation of energies in the combined CBS and thermodynamic limits. See the SI for precise details about our composite corrections.

Equation of state. In Fig. 3, we show the equation of state (EOS) of Li and Al as a function of the cell volume, where the cohesive energy, which is defined with respect to a single atom, was counterpoise-corrected by surrounding the atom with ghost atoms and their basis functions.[67,73,74] Single-atom calculations were performed in a spin-unrestricted manner. For Al, in sequential calculations from small to large volumes, we found that using the converged HF density matrix of the previous volume was essential in obtaining a smooth curve. The HF EOS was calculated by performing TDL extrapolation at each lattice constant. The correlation energy contribution to

Table 1: Lattice constant a, bulk modulus B, and cohesive energy E_{coh} of lithium and aluminum. All experimental (Exp.) values have been corrected for zero-point motion (ZPM) effects as described in the text. The HF cohesive energy of Li reported in Ref. 67 includes a ZPM correction, which we estimate to be only 0.001 E_h.

	a (Å)	B (GPa)	E_{coh} (E_h/atom)
Li			
HF (ours)	3.68	9.0	−0.022
HF[67]	3.73	8.1-11.9	−0.020
CCSD (ours)	3.49	12.8	−0.051
Incremental CCSD[32]	3.50	–	−0.060
CCSD(T)$_{\mathrm{SR}}$	3.48	12.9	−0.054
CCSD-SVC	3.49	12.7	−0.057
Exp.[65,68–70]	3.45	13.3	−0.061
Al			
HF	4.08	80.0	−0.051
CCSD	4.02	93.2	−0.109
CCSD(T)$_{\mathrm{SR}}$	4.02	91.7	−0.114
CCSD-SVC	4.03	91.4	−0.123
Exp.[65,70–72]	4.02	80.3	−0.126

the CCSD EOS was either TDL extrapolated with smaller meshes (Li) or calculated using our largest $\boldsymbol{k}$-point meshes (Al) and then rigidly shifted by a finite-size correction calculated at lattice parameters 3.5 Å (Li) and 4.05 Å (Al), which are close to the experimental values. See SI for further details.

In Fig. 3(a) and (b), we show CCSD results in the QZ basis and CBS limit, which only differ by about 0.2 mE_h for Li and 1-2 mE_h for Al, indicating the good performance of our optimized basis sets. By fitting our data to a Birch-Murnaghan equation,[64,65] we extract the lattice constant, bulk modulus, and cohesive energy. These properties are listed in Tab. 1 and compared to experimental values. The experimental results have been corrected for zero-point motion (ZPM) using the correction obtained in Ref. 65 with the HSE06 functional,[75–77] although other functionals yield similar corrections.

Beyond coupled cluster with single and double excitations. Comparing to experiment, we find that the magnitude of the CCSD cohesive energy is too small by about 10 mE_h (Li) and 20 mE_h (Al), which our testing suggests is mostly due to insufficient correlation in the solid rather than the

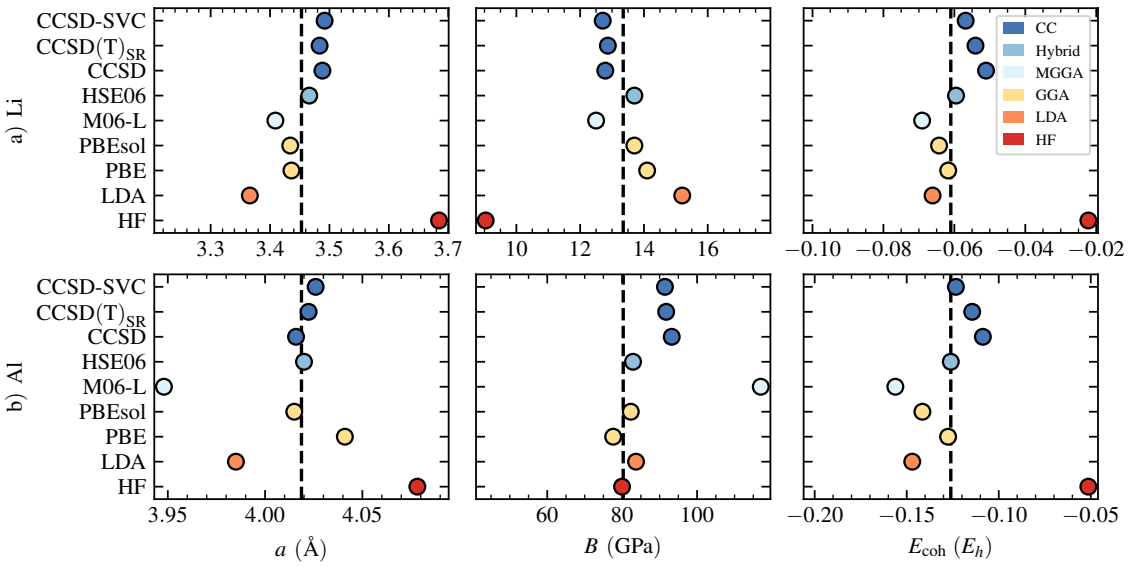

Figure 4: Structural properties (lattice parameter a, bulk modulus B, and cohesive energy E_{coh}) of (a) lithium and (b) aluminum evaluated with HF (this work), DFT (from Ref. 65) colored by rung, and coupled cluster (CC) (this work) in its CCSD, CCSD(T)$_{\mathrm{SR}}$ and UEG scaled CCSD (CCSD-SVC) forms. The zero or low temperature experimental values (from Refs. 65,68–72) are shown by dashed vertical lines. All experimental (Exp.) values have been corrected for zero-point motion (ZPM) effects as described in the text.

single atom. Therefore, we developed and applied two approximate improvements to CCSD. First, we test CCSD(T), which applies a perturbative correction to the correlation energy due to triple excitations. The energy of the atom was calculated in the usual manner, but the CCSD(T) energy of the solid must be calculated in a modified form because otherwise it diverges in the TDL[17] due to the contribution of low-energy excitations with vanishing momentum transfer. Because the long-range part of the Coulomb interaction is already treated with CCSD (which treats density fluctuations at the level of the random-phase approximation[78–82]), we only consider the CCSD(T) correlation energy due to the short-range part of the Coulomb interaction. In practice, we calculate the CCSD(T) correlation energy using a coarse $\boldsymbol{k}$-point mesh, which can be understood as an approximate regularization of an infrared divergence via enforcement of a minimum momentum transfer determined by the employed $\boldsymbol{k}$-point mesh; we will refer to this method as CCSD(T)$_{\mathrm{SR}}$. Here we use $N_{\boldsymbol{k}} = 2^3$ for Li and $N_{\boldsymbol{k}} = 2\times2\times1$ for Al, which corresponds to neglecting momentum transfers that are less than about 1 Å^{-1}. This (T) contribution is evaluated at the QZ level indepen-

dent from basis set studied. The EOS using this approach is shown in the middle panels of Fig. 3, with properties given in Tab. 1. The error in the cohesive energy is reduced by about 30%. Other properties are also improved, but less significantly. Clearly, these results are dependent on the choice of the coarse $\boldsymbol{k}$-point mesh, and future work will investigate a black-box determination. For example, the density-dependent Thomas-Fermi screening length can help identify an appropriate coarse $\boldsymbol{k}$-point mesh or a similarly screened Coulomb potential can be used in the evaluation of the (T) contribution.[17]

For our second approximate improvement to CCSD, we recall that valence electrons in simple metals are delocalized and thus reasonably approximated as a UEG. The relative simplicity of the UEG enabled its numerically exact ground-state solution by diffusion Monte Carlo,[83] which paved the way for the local density approximation and the subsequent family of functionals that are exact in the limit of uniform density. In contrast, CCSD is not exact in this limit, but the availability of numerical data on the UEG suggests a straightforward correction. In this approach, which we refer to as CCSD with scaling valence correlation (CCSD-SVC),[84] we calculate the correlation energy of the solid as

$$E_{\mathrm{c}}^{\mathrm{CCSD\text{-}SVC}} = E_{\mathrm{c,core}}^{\mathrm{CCSD}} + E_{\mathrm{c,val}}^{\mathrm{CCSD}}/F(\rho), \tag{2}$$

where $E_{\mathrm{c,core/val}}$ is the correlation energy of the core/valence electrons, and $F(\rho)$ is a non-empirical factor that is determined according to the UEG of the same valence density ρ as the sytem under study. Specifically, we take $F(\rho) = e_{\mathrm{c}}^{\mathrm{CCSD}}(\rho)/e_{\mathrm{c}}^{\mathrm{exact}}(\rho)$, where $e_{\mathrm{c}}^{\mathrm{exact}}$ is the exact correlation energy density of the UEG according to the Perdew-Zunger fit[85] to diffusion Monte Carlo results[83] and $e_{\mathrm{c}}^{\mathrm{CCSD}}$ is the CCSD correlation energy density of the UEG according to our own Perdew-Zunger-style fit to CCSD results from Shepherd.[28] By construction, the CCSD-SVC correlation energy is exact in the limit of uniform density, suggesting an improved applicability to atomistic simple metals. For this UEG description, we consider one valence electron for Li and three valence electrons for Al, and we calculate the density at all lattice parameters studied. At the experimental lattice parameters, this approach gives valence densities corresponding to Wigner-Seitz radii of about $r_s = 3.24$ Bohr for Li and $r_s = 2.06$ Bohr for Al and scaling factors $F \approx 0.8$–0.9. For

Li, we calculate $E_{\mathrm{c,val}}^{\mathrm{CCSD}}$ by performing calculations with the $1s$ electrons frozen and then define $E_{\mathrm{c,core}}^{\mathrm{CCSD}} = E_{\mathrm{c}}^{\mathrm{CCSD}} - E_{\mathrm{c,val}}^{\mathrm{CCSD}}$, where $E_{\mathrm{c}}^{\mathrm{CCSD}}$ is calculated by correlating both core and valence electrons. For Al, $E_{\mathrm{c,core}}^{\mathrm{CCSD}} = 0$ because the $1s$, $2s$, and $2p$ electrons are treated by the pseudopotential. The EOS calculated using CCSD-SVC is shown in the bottom row of Fig. 3, with properties given in Tab. 1. The cohesive energies are significantly improved over CCSD or CCSD(T)$_{\mathrm{SR}}$, only deviating by 3-4 mE_h from experiment. Overall, CCSD-SVC predicts lattice parameters and bulk moduli that are similar to those of CCSD or CCSD(T)$_{\mathrm{SR}}$.

Discussion. For Li, our results can be compared to previous ones in the literature, which are included in Tab. 1. First, our HF results are in good agreement with those reported in Ref. 67, which were calculated using an optimized DZ basis with the CRYSTAL package.[86] This agreement confirms a consistent starting point for correlated calculations. To our knowledge, there are no reports of periodic CCSD calculations of the equation of state of BCC Li (a recent work[34] used periodic CCSD to estimate the energy difference between FCC and BCC Li). However, in Ref. 32, an incremental CCSD scheme was applied based on finite clusters. Although that work found a lattice constant in good agreement with ours, it found a cohesive energy that was significantly different (-0.060 E_h compared to our -0.051 E_h) and in much better agreement with experiment. As discussed in detail in that work, the application of incremental schemes to metallic systems is delicate and nontrivial, and this might be responsible for the disagreement. Based on our investigations, we find no evidence for errors on the order of 0.01 E_h. Instead, we believe that this level of accuracy is expected for CCSD based on its known performance for the UEG,[18,28] where it underestimates the correlation energy at metallic densities by about 10-20%.

Finally, it is natural to compare CC methods to DFT, which is significantly more affordable. In Fig. 4, we compare the properties of Li and Al predicted by CCSD, CCSD(T)$_{\mathrm{SR}}$, and CCSD-SVC to those predicted by HF and by common functionals, as reported in Ref. 65. We compare to a few popular functionals of increasing sophistication, including the local density approximation (LDA),[15] the generalized gradient approximations (GGAs) PBE[87] and PBEsol,[88] the meta GGA M06-L,[89] and the screened hybrid HSE06.[75–77] Overall, the CC results are comparable to

those from GGAs but worse than the hybrid HSE06, which performs extremely well for these two materials.

Looking forward, it will be interesting to apply CC methods to transition metals and to less uniform metallic systems, such as metal surfaces including adsorbates or chemical reactants. For these latter problems, we expect to see an increased advantage of CC over DFT, due to the greater variations in the electron density and the importance of dispersion interactions. More broadly, our work has reemphasized the need for wavefunction based methods that improve upon CCSD without the use of perturbation theories that diverge for metals. Beyond more systematic investigation of the two methods proposed here, other possibilities include the use of spin-component scaling,[90–92] regularization,[93–95] or screened interactions,[17,96] although these approaches typically introduce empirical parameters. Alternatively, the full or limited inclusion of non-perturbative triple excitations[97–99] is a promising *ab initio* route towards chemical accuracy in metallic solids.

Associated content

Supporting Information

The Supporting Information is available free of charge at [publisher inserts link].

Further details on composite corrections, pseudopotentials, single atom calculations, and basis set effects (PDF).

Author information

[publisher inserts author information]

Notes

The authors declare no competing financial interests.

Acknowledgement

This work was primarily supported by the Columbia Center for Computational Electrochemistry (V.A.N.) and partially supported by the National Science Foundation under Grant Numbers OAC-1931321 (H.-Z.Y.) and CHE-1848369 (T.C.B.). We acknowledge computing resources from Columbia University's Shared Research Computing Facility project, which is supported by NIH Research Facility Improvement Grant 1G20RR030893-01, and associated funds from the New York State Empire State Development, Division of Science Technology and Innovation (NYSTAR) Contract C090171, both awarded April 15, 2010. Some calculations were performed using resources provided by the Flatiron Institute. The Flatiron Institute is a division of the Simons Foundation. Matplotlib,[100] NumPy,[101] pandas,[102] SciPy,[103] seaborn,[104] and ColorBrewer[105] were used for calculations, analysis, and visualization.

References

(1) Hirata, S.; Podeszwa, R.; Tobita, M.; Bartlett, R. J. Coupled-cluster singles and doubles for extended systems. *J. Chem. Phys.* **2004**, *120*, 2581–2592.

(2) Marsman, M.; Grüneis, A.; Paier, J.; Kresse, G. Second-order Møller–Plesset perturbation theory applied to extended systems. I. Within the projector-augmented-wave formalism using a plane wave basis set. *J. Chem. Phys.* **2009**, *130*, 184103.

(3) Grüneis, A.; Marsman, M.; Kresse, G. Second-order Møller–Plesset perturbation theory applied to extended systems. II. Structural and energetic properties. *J. Chem. Phys.* **2010**, *133*, 074107.

(4) Booth, G. H.; Grüneis, A.; Kresse, G.; Alavi, A. Towards an exact description of electronic wavefunctions in real solids. *Nature* **2013**, *493*, 365–370.

(5) Liao, K.; Grüneis, A. Communication: Finite size correction in periodic coupled cluster theory calculations of solids. *J. Chem. Phys.* **2016**, *145*, 141102.

(6) McClain, J.; Sun, Q.; Chan, G. K.-L.; Berkelbach, T. C. Gaussian-based coupled-cluster theory for the ground-state and band structure of solids. *J. Chem. Theory Comput.* **2017**, *13*, 1209–1218.

(7) Gruber, T.; Liao, K.; Tsatsoulis, T.; Hummel, F.; Grüneis, A. Applying the coupled-cluster ansatz to solids and surfaces in the thermodynamic limit. *Phys. Rev. X* **2018**, *8*, 021043.

(8) Hummel, F. Finite temperature coupled cluster theories for extended systems. *J. Chem. Theory Comput.* **2018**, *14*, 6505–6514.

(9) Liao, K.; Li, X.-Z.; Alavi, A.; Grüneis, A. A comparative study using state-of-the-art electronic structure theories on solid hydrogen phases under high pressures. *npj Comput. Mater.* **2019**, *5*, 1–6.

(10) Azadi, S.; Booth, G. H.; Kühne, T. D. Equation of state of atomic solid hydrogen by stochastic many-body wave function methods. *J. Chem. Phys.* **2020**, *153*, 204107.

(11) Gao, Y.; Sun, Q.; Yu, J. M.; Motta, M.; McClain, J.; White, A. F.; Minnich, A. J.; Chan, G. K.-L. Electronic structure of bulk manganese oxide and nickel oxide from coupled cluster theory. *Phys. Rev. B* **2020**, *101*, 165138.

(12) Lange, M. F.; Berkelbach, T. C. Active space approaches combining coupled-cluster and perturbation theory for ground states and excited states. *Mol. Phys.* **2020**, e1808726.

(13) Pulkin, A.; Chan, G. K.-L. First-principles coupled cluster theory of the electronic spectrum of transition metal dichalcogenides. *Phys. Rev. B* **2020**, *101*, 241113(R).

(14) Hohenberg, P.; Kohn, W. Inhomogeneous electron gas. *Phys. Rev.* **1964**, *136*, B864–B871.

(15) Kohn, W.; Sham, L. J. Self-consistent equations including exchange and correlation effects. *Phys. Rev.* **1965**, *140*, A1133–A1138.

(16) Macke, W. Über die Wechselwirkungen im Fermi-Gas. Polarisationserscheinungen, Correlationsenergie, Elektronenkondensation. *Z. Naturforsch. A* **1950**, *5*, 192–208, Publisher: De Gruyter.

(17) Shepherd, J. J.; Grüneis, A. Many-body quantum chemistry for the electron gas: Convergent perturbative theories. *Phys. Rev. Lett.* **2013**, *110*, 226401.

(18) Callahan, J. M.; Lange, M. F.; Berkelbach, T. C. Dynamical correlation energy of metals in large basis sets from downfolding and composite approaches. *J. Chem. Phys.* **2021**, *154*, 211105.

(19) Bartlett, R. J.; Musiał, M. Coupled-cluster theory in quantum chemistry. *Rev. Mod. Phys.* **2007**, *79*, 291–352.

(20) Gell-Mann, M.; Brueckner, K. A. Correlation energy of an electron gas at high density. *Phys. Rev.* **1957**, *106*, 364–368.

(21) Bishop, R. F.; Lührmann, K. H. Electron correlations: I. Ground-state results in the high-density regime. *Phys. Rev. B* **1978**, *17*, 3757–3780.

(22) Bishop, R. F.; Lührmann, K. H. Electron correlations. II. Ground-state results at low and metallic densities. *Phys. Rev. B* **1982**, *26*, 5523–5557.

(23) Shepherd, J. J.; Henderson, T. M.; Scuseria, G. E. Range-separated Brueckner coupled cluster doubles theory. *Phys. Rev. Lett.* **2014**, *112*, 133002.

(24) Irmler, A.; Gallo, A.; Hummel, F.; Grüneis, A. Duality of ring and ladder diagrams and its importance for many-electron perturbation theories. *Phys. Rev. Lett.* **2019**, *123*, 156401.

(25) Freeman, D. L. Coupled-cluster expansion applied to the electron gas: Inclusion of ring and exchange effects. *Phys. Rev. B* **1977**, *15*, 5512–5521.

(26) Shepherd, J. J.; Grüneis, A.; Booth, G. H.; Kresse, G.; Alavi, A. Convergence of many-body wave-function expansions using a plane-wave basis: From homogeneous electron gas to solid state systems. *Phys. Rev. B* **2012**, *86*, 035111.

(27) Shepherd, J. J.; Henderson, T. M.; Scuseria, G. E. Coupled cluster channels in the homogeneous electron gas. *J. Chem. Phys.* **2014**, *140*, 124102.

(28) Shepherd, J. J. Communication: Convergence of many-body wave-function expansions using a plane-wave basis in the thermodynamic limit. *J. Chem. Phys.* **2016**, *145*, 031104.

(29) Neufeld, V. A.; Thom, A. J. W. A study of the dense uniform electron gas with high orders of coupled cluster. *J. Chem. Phys.* **2017**, *147*, 194105.

(30) Mihm, T. N.; McIsaac, A. R.; Shepherd, J. J. An optimized twist angle to find the twist-averaged correlation energy applied to the uniform electron gas. *J. Chem. Phys.* **2019**, *150*, 191101.

(31) Liao, K.; Schraivogel, T.; Luo, H.; Kats, D.; Alavi, A. Towards efficient and accurate *ab initio* solutions to periodic systems via transcorrelation and coupled cluster theory. *Phys. Rev. Res.* **2021**, *3*, 033072.

(32) Stoll, H.; Paulus, B.; Fulde, P. An incremental coupled-cluster approach to metallic lithium. *Chem. Phys. Lett.* **2009**, *469*, 90–93.

(33) Voloshina, E.; Paulus, B. Development of a wavefunction-based ab initio method for metals applying the method of increments. *Z. Phys. Chem.* **2010**, *224*, 369–381.

(34) Mihm, T. N.; Schäfer, T.; Ramadugu, S. K.; Weiler, L.; Grüneis, A.; Shepherd, J. J. A shortcut to the thermodynamic limit for quantum many-body calculations of metals. *Nat. Comput. Sci.* **2021**, *1*, 801–808.

(35) Weiler, L.; Mihm, T.; Shepherd, J. J. Machine learning for a finite size correction in periodic coupled cluster theory calculations. *J. Chem. Phys.* **2022**, 5.0086580.

(36) Boys, S. Electronic wave functions - I. A general method of calculation for the stationary states of any molecular system. *Proc. R. Soc. Lond. A* **1950**, *200*, 542–554.

(37) VandeVondele, J.; Hutter, J. Gaussian basis sets for accurate calculations on molecular systems in gas and condensed phases. *J. Chem. Phys.* **2007**, *127*, 114105.

(38) Raghavachari, K.; Trucks, G. W.; Pople, J. A.; Head-Gordon, M. A fifth-order perturbation comparison of electron correlation theories. *Chem. Phys. Lett.* **1989**, *157*, 479–483.

(39) Sun, Q.; Berkelbach, T. C.; Blunt, N. S.; Booth, G. H.; Guo, S.; Li, Z.; Liu, J.; McClain, J. D.; Sayfutyarova, E. R.; Sharma, S.; Wouters, S.; Chan, G. K.-L. PySCF: the Python-based simulations of chemistry framework. *WIREs Comput. Mol. Sci.* **2018**, *8*, e1340.

(40) Sun, Q. et al. Recent developments in the PySCF program package. *J. Chem. Phys.* **2020**, *153*, 024109.

(41) Sun, Q. Libcint: An efficient general integral library for Gaussian basis functions. *J. Comput. Chem.* **2015**, *36*, 1664–1671.

(42) Sun, Q.; Berkelbach, T. C.; McClain, J. D.; Chan, G. K.-L. Gaussian and plane-wave mixed density fitting for periodic systems. *J. Chem. Phys.* **2017**, *147*, 164119.

(43) Ye, H.-Z.; Berkelbach, T. C. Fast periodic Gaussian density fitting by range separation. *J. Chem. Phys.* **2021**, *154*, 131104.

(44) Ye, H.-Z.; Berkelbach, T. C. Tight distance-dependent estimators for screening two-center and three-center short-range Coulomb integrals over Gaussian basis functions. *J. Chem. Phys.* **2021**, *155*, 124106.

(45) Goedecker, S.; Teter, M.; Hutter, J. Separable dual-space Gaussian pseudopotentials. *Phys. Rev. B* **1996**, *54*, 1703–1710, Number: 3.

(46) Hartwigsen, C.; Goedecker, S.; Hutter, J. Relativistic separable dual-space Gaussian pseudopotentials from H to Rn. *Phys. Rev. B* **1998**, *58*, 3641–3662.

(47) CP2K CP2K code. https://github.com/cp2k/cp2k, accessed 14th Jan 2022.

(48) Hutter, J. New optimization of GTH pseudopotentials for PBE, SCAN, PBE0 functionals. GTH pseudopotentials for Hartree-Fock. NLCC pseudopotentials for PBE. https://github.com/juerghutter/GTH, accessed 14th Jan 2022.

(49) Daga, L. E.; Civalleri, B.; Maschio, L. Gaussian basis sets for crystalline solids: All-purpose basis set libraries vs system-specific optimizations. *J. Chem. Theory Comput.* **2020**, *16*, 2192–2201.

(50) Morales, M. A.; Malone, F. D. Accelerating the convergence of auxiliary-field quantum Monte Carlo in solids with optimized Gaussian basis sets. *J. Chem. Phys.* **2020**, *153*, 194111.

(51) Li, W.-L.; Chen, K.; Rossomme, E.; Head-Gordon, M.; Head-Gordon, T. Optimized pseudopotentials and basis sets for semiempirical density functional theory for electrocatalysis applications. *J. Phys. Chem. Lett.* **2021**, *12*, 10304–10309.

(52) Zhou, Y.; Gull, E.; Zgid, D. Material-specific optimization of Gaussian basis sets against plane wave data. *J. Chem. Theor. Comput.* **2021**, *17*, 5611–5622.

(53) Møller, C.; Plesset, M. S. Note on an approximation treatment for many-electron systems. *Phys. Rev.* **1934**, *46*, 618–622.

(54) Monkhorst, H. J.; Pack, J. D. Special points for Brillouin-zone integrations. *Phys. Rev. B* **1976**, *13*, 5188–5192.

(55) Booth, G. H.; Tsatsoulis, T.; Chan, G. K.-L.; Grüneis, A. From plane waves to local Gaussians for the simulation of correlated periodic systems. *J. Chem. Phys.* **2016**, *145*, 084111.

(56) Ye, H.-Z.; Berkelbach, T. C. Correlation-consistent Gaussian basis sets for solids made simple. *J. Chem. Theor. Comput.* **2022**, *18*, 1595–1606.

(57) Baldereschi, A. Mean-value point in the Brillouin zone. *Physical Review B* **1973**, *7*, 5212–5215.

(58) Chadi, D. J.; Cohen, M. L. Special points in the Brillouin zone. *Phys. Rev. B* **1973**, *8*, 5747–5753.

(59) Rajagopal, G.; Needs, R. J.; James, A.; Kenny, S. D.; Foulkes, W. M. C. Variational and diffusion quantum Monte Carlo calculations at nonzero wave vectors: Theory and application to diamond-structure germanium. *Phys. Rev. B* **1995**, *51*, 10591–10600.

(60) Lin, C.; Zong, F. H.; Ceperley, D. M. Twist-averaged boundary conditions in continuum quantum Monte Carlo algorithms. *Phys. Rev. E* **2001**, *64*, 016702.

(61) Morris, A. J.; Pickard, C. J.; Needs, R. J. Hydrogen/silicon complexes in silicon from computational searches. *Phys. Rev. B* **2008**, *78*, 184102.

(62) Paier, J.; Hirschl, R.; Marsman, M.; Kresse, G. The Perdew–Burke–Ernzerhof exchange-correlation functional applied to the G2-1 test set using a plane-wave basis set. *J. Chem. Phys.* **2005**, *122*, 234102.

(63) Sundararaman, R.; Arias, T. A. Regularization of the Coulomb singularity in exact exchange by Wigner-Seitz truncated interactions: Towards chemical accuracy in nontrivial systems. *Phys. Rev. B* **2013**, *87*, 165122.

(64) Birch, F. Finite elastic strain of cubic crystals. *Phys. Rev.* **1947**, *71*, 809–824.

(65) Zhang, G.-X.; Reilly, A. M.; Tkatchenko, A.; Scheffler, M. Performance of various density-functional approximations for cohesive properties of 64 bulk solids. *New J. Phys.* **2018**, *20*, 063020.

(66) Helgaker, T.; Klopper, W.; Koch, H.; Noga, J. Basis-set convergence of correlated calculations on water. *J. Chem. Phys.* **1997**, *106*, 9639–9646.

(67) Paulus, B.; Rosciszewski, K. Hartree–Fock ground-state properties for the group 1 alkali metals and the group 11 noble metals. *J. Phys. Condens. Matter* **2007**, *19*, 346217.

(68) Felice, R. A.; Trivisonno, J.; Schuele, D. E. Temperature and pressure dependence of the single-crystal elastic constants of Li 6 and natural lithium. *Phys. Rev. B* **1977**, *16*, 5173–5184.

(69) Berliner, R.; Werner, S. A. Effect of stacking faults on diffraction: The structure of lithium metal. *Phys. Rev. B* **1986**, *34*, 3586–3603.

(70) Kittel, C. *Introduction to solid state physics*, 8th ed.; John Wiley & Sons, Inc., 2005.

(71) Kamm, G. N.; Alers, G. A. Low-temperature elastic moduli of aluminum. *J. Appl. Phys.* **1964**, *35*, 327–330.

(72) Giri, A. K.; Mitra, G. B. Extrapolated values of lattice constants of some cubic metals at absolute zero. *J. Phys. D: Appl. Phys.* **1985**, *18*, L75–L78.

(73) Boys, S.; Bernardi, F. The calculation of small molecular interactions by the differences of separate total energies. Some procedures with reduced errors. *Mol. Phys.* **1970**, *19*, 553–566.

(74) van Duijneveldt, F. B.; van Duijneveldt-van de Rijdt, J. G. C. M.; van Lenthe, J. H. State of the art in counterpoise theory. *Chem. Rev.* **1994**, *94*, 1873–1885.

(75) Heyd, J.; Scuseria, G. E.; Ernzerhof, M. Hybrid functionals based on a screened Coulomb potential. *J. Chem. Phys.* **2003**, *118*, 8207–8215.

(76) Heyd, J.; Scuseria, G. E.; Ernzerhof, M. Erratum: "Hybrid functionals based on a screened Coulomb potential" [J. Chem. Phys. 118, 8207 (2003)]. *J. Chem. Phys.* **2006**, *124*, 219906.

(77) Krukau, A. V.; Vydrov, O. A.; Izmaylov, A. F.; Scuseria, G. E. Influence of the exchange screening parameter on the performance of screened hybrid functionals. *J. Chem. Phys.* **2006**, *125*, 224106.

(78) Bohm, D.; Pines, D. A collective description of electron interactions. I. Magnetic interactions. *Phys. Rev.* **1951**, *82*, 625–634.

(79) Pines, D.; Bohm, D. A collective description of electron interactions: II. Collective vs individual particle aspects of the interactions. *Phys. Rev.* **1952**, *85*, 338–353.

(80) Bohm, D.; Pines, D. A collective description of electron interactions: III. Coulomb interactions in a degenerate electron gas. *Phys. Rev.* **1953**, *92*, 609–625.

(81) Pines, D. A collective description of electron interactions: IV. Electron interaction in metals. *Phys. Rev.* **1953**, *92*, 626–636.

(82) Scuseria, G. E.; Henderson, T. M.; Sorensen, D. C. The ground state correlation energy of the random phase approximation from a ring coupled cluster doubles approach. *J. Chem. Phys.* **2008**, *129*, 231101.

(83) Ceperley, D. M.; Alder, B. J. Ground state of the electron gas by a stochastic method. *Phys. Rev. Lett.* **1980**, *45*, 566–569.

(84) Gordon, M. S.; Truhlar, D. G. Scaling all correlation energy in perturbation theory calculations of bond energies and barrier heights. *J. Am. Chem. Soc.* **1986**, *108*, 5412–5419.

(85) Perdew, J. P.; Zunger, A. Self-interaction correction to density-functional approximations for many-electron systems. *Phys. Rev. B* **1981**, *23*, 5048–5079.

(86) Saunders, V. R.; Dovesi, R.; Roetti, C.; Orlando, R.; Zicowich-Wilson, C. M.; Harrison, N. M.; Doll, K.; Civalleri, B.; Bush, I. J.; D'Arco, P.; Llunell, M. CRYSTAL2003. 2004; University of Torino, Torino.

(87) Perdew, J. P.; Burke, K.; Ernzerhof, M. Generalized gradient approximation made simple. *Phys. Rev. Lett.* **1996**, *77*, 3865–3868.

(88) Perdew, J. P.; Ruzsinszky, A.; Csonka, G. I.; Vydrov, O. A.; Scuseria, G. E.; Constantin, L. A.; Zhou, X.; Burke, K. Restoring the density-gradient expansion for exchange in solids and surfaces. *Phys. Rev. Lett.* **2008**, *100*, 136406.

(89) Zhao, Y.; Truhlar, D. G. A new local density functional for main-group thermochemistry, transition metal bonding, thermochemical kinetics, and noncovalent interactions. *J. Chem. Phys.* **2006**, *125*, 194101.

(90) Grimme, S. Improved second-order Møller–Plesset perturbation theory by separate scaling of parallel- and antiparallel-spin pair correlation energies. *J. Chem. Phys.* **2003**, *118*, 9095–9102.

(91) Takatani, T.; Hohenstein, E. G.; Sherrill, C. D. Improvement of the coupled-cluster singles and doubles method via scaling same- and opposite-spin components of the double excitation correlation energy. *J. Chem. Phys.* **2008**, *128*, 124111.

(92) Grimme, S.; Goerigk, L.; Fink, R. F. Spin-component-scaled electron correlation methods. *WIREs Comput Mol Sci* **2012**, *2*, 886–906.

(93) Lee, J.; Head-Gordon, M. Regularized orbital-optimized second-order Møller–Plesset perturbation Theory: A reliable fifth-order-scaling electron correlation model with orbital energy dependent regularizers. *J. Chem. Theor. Comput.* **2018**, *14*, 5203–5219.

(94) Shee, J.; Loipersberger, M.; Rettig, A.; Lee, J.; Head-Gordon, M. Regularized second-order Møller–Plesset theory: A more accurate alternative to conventional MP2 for noncovalent interactions and transition metal thermochemistry for the same computational cost. *J. Phys. Chem. Lett.* **2021**, *12*, 12084–12097.

(95) Keller, E.; Tsatsoulis, T.; Reuter, K.; Margraf, J. T. Regularized second-order correlation methods for extended systems. *J. Chem. Phys.* **2022**, *156*, 024106.

(96) Landsberg, P. T. A contribution to the theory of soft X-ray emission bands of sodium. *Proc. Phys. Soc. A* **1949**, *62*, 806–816.

(97) Lee, Y. S.; Kucharski, S. A.; Bartlett, R. J. A coupled cluster approach with triple excitations. *J. Chem. Phys.* **1984**, *81*, 5906–5912.

(98) Urban, M.; Noga, J.; Cole, S. J.; Bartlett, R. J. Towards a full CCSDT model for electron correlation. *J. Chem. Phys.* **1985**, *83*, 4041–4046.

(99) Shavitt, I.; Bartlett, R. J. *Many-body methods in chemistry and physics: MBPT and coupled-cluster theory*; Cambridge Molecular Science; Cambridge University Press: Cambridge, 2009.

(100) Hunter, J. D. Matplotlib: A 2D graphics environment. *Comput. Sci. Eng.* **2007**, *9*, 90–95.

(101) Harris, C. R. et al. Array programming with NumPy. *Nature* **2020**, *585*, 357–362.

(102) McKinney, W. Data structures for statistical computing in python. Proceedings of the 8th Python in Science Conference. 2009; pp 55 – 61.

(103) SciPy 1.0 Contributors et al. SciPy 1.0: fundamental algorithms for scientific computing in Python. *Nature Methods* **2020**, *17*, 261–272.

(104) Waskom, M. L. seaborn: statistical data visualization. *J. Open Source Softw.* **2021**, *6*, 3021.

(105) Brewer, C.; Harrower, M.; Sheesley, B.; Woodruff, A.; Heyman, D. ColorBrewer2. https://colorbrewer2.org/, accessed 25th Mar 2022.